Ab Initio and RRKM Studies of the Reactions of C, CH, and $^1CH_2$ with Acetylene

Renee Guadagnini and George C. Schatz*

Department of Chemistry, Northwestern University, Evanston, Illinois 60208-3113

Stephen P. Walch

Thermosciences Institute, MS 230-3, NASA Ames Research Center, Moffett Field, California 94035-1000
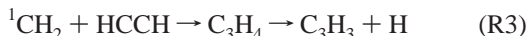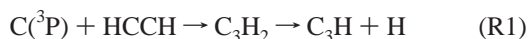
Received: February 11, 1998

We present ab initio calculations of geometries, energies, and normal mode frequencies for complexes and saddle points along the minimum energy reaction path for the reaction $C + HCCH \rightarrow C_3H_2 \rightarrow C_3H + H$. We also present ab initio calculations along the minimum energy reaction path in the entrance channel for the reactions $C + HCCH$, $CH + HCCH$, and $^1CH_2 + HCCH$. These results and those presented earlier by Walch[1] are used to calculate rate constants for the reactions of C, CH, and $^1CH_2$ with acetylene, using variational RRKM theory. The rate constants obtained agree well with experimental results for all three reactions. Unimolecular lifetimes for intermediate complexes associated with each reaction path are also presented. Among the more stable C_3 isomers are propargyl and propargylene, which have lifetimes of 25 and 1900 ps, respectively, under thermal reaction conditions.

I. Introduction

Radical species and molecules containing three carbon atoms and one to four hydrogen atoms have been of significant interest recently in hydrocarbon combustion[1−3] and interstellar chemistry.[4,5] Many of these species are believed to be important precursors to soot formation[6] and in particular may be involved in the formation of benzene and other C_6 species through dimerization reactions.[1,2] However, there is still some question whether mechanisms involving C_3 species can compete with other mechanisms, such as those involving $n\text{-}C_4H_3$ or ion−molecule reactions, in the formation of aromatics.[7,8]

In this paper, we present a study of three radical reactions with acetylene that are possible sources of C_3 molecules.[1,2,9] The reactions are

$$C(^3P) + HCCH \rightarrow C_3H_2 \rightarrow C_3H + H \qquad (R1)$$

$$CH(X^2\Pi) + HCCH \rightarrow C_3H_3 \rightarrow C_3H_2 + H \qquad (R2)$$

$$^1CH_2 + HCCH \rightarrow C_3H_4 \rightarrow C_3H_3 + H \qquad (R3)$$

We use variational RRKM theory with ab initio potential surface data to determine the rates of these reactions and the lifetimes of intermediates. The results will be useful for interpreting kinetic measurements and in kinetic modeling of combustion processes.

Previous work has reported ab initio results for all three reactions,[1,4,10−12] although in none of these studies has enough information been presented to determine rate constants from RRKM theory. Walch[1] has presented information about the saddle points and minima associated with reactions R2 and R3 at a level that is comparable to that considered here, so we use his results as much as possible. Missing in this work was information about the minimum energy path for the initial addition step (the rate-limiting step under most circumstances), so we present new results here for R2 and R3 concerning this.

Earlier studies of R1 did not report quantitative reaction path information,[4,10−12] so new ab initio calculations of barriers along the reaction paths for R1 and of the minimum energy path for the initial addition step are described in this paper. This information is used to perform variational RRKM calculations to determine rate constants and lifetimes.

Part II of this paper gives details and results from the ab initio reaction path calculations. Part III details the RRKM calculations. The results are discussed in part IV.

II. Reaction Path Calculations

The ab initio calculations follow the basic procedure outlined in ref 1. Briefly, we performed complete active space self consistent field (CASSCF) gradient calculations to locate the stationary points, then internally contracted configuration interaction (ICCI) calculations to determine accurate energies without reoptimizing the geometries. The CASSCF calculations used a polarized valence double-zeta basis set from Dunning and Hay, augmented with a single set of 3d functions on each carbon and a single set of 2p functions on each hydrogen. The ICCI calculations used the Dunning correlation consistent polarized triple-zeta basis set, but without the f functions on C or the d functions on H. Results of the calculations are presented in Tables 1−9 and Figure 1. Further details of the ab initio calculations will be presented elsewhere.[13]

Stationary point energies, moments of inertia, and frequencies for R1 are presented in Tables 1 and 2. We have used simple abbreviated names for the species, but we note for completeness that in Table 1 min1 is *s-trans*-propenediylidene, min2 is *s-cis*-propenediylidene, min3 is propargylene, min4 is cyclopropenylidene, and min5 is vinylidenecarbene. A schematic drawing of the reaction path is shown in Figure 1a. Only triplet surfaces have been considered, as reaction is expected to be quite efficient for these barrierless spin-allowed pathways (as discussed further below). Note that there are two possible products of R1, linear and cyclic C_3H (propynylidyne and

TABLE 1: Energies, Frequencies, and Moments of Inertia for Minima for C + HCCH

	reactant	min1	min2	min3	min4 cyclic	min5 propargylene	lin C_3H	cyc C_3H	cyclic singlet
Structure									
Energy (kcal/mol)	0.0	-29.0	-27.3	-83.9	-45.3	-57.0	1.6	2.0	-93.6
harmonic frequencies (cm^{-1})	3627	3399	3405	3588	3480	3391	3580	3454	3425
	1977	3323	3266	3477	3299	3092	1836	1699	3185
	774	1353	1430	1643	1619	1923	1118	1108	1615
	774	1132	1109	1116	1042	1496	765	965	1356
	3550	1100	1060	667	1036	159	265	848	1009
	634	921	909	470	954	1003	391	843	974
	634	277	305	328	901	183	217		859
		742	685	404	645	637			955
		498	401	262	626	366			774
moments of inertia ($10^5\ m_ea_0{}^2$)		0.535	0.357	0.3031	1.061	0.256	0.215	0.941	
		3.298	3.548	4.460	1.351	4.018	4.342	2.406	
		3.833	3.904	4.763	2.292	4.274	4.557	3.348	

TABLE 2: Energies, Frequencies, and Moments of Inertia for Saddle Points for C + HCCH

	path	sp1	sp2	sp3	sp4	sp5	sp6
Structure							
Energy (kcal/mol)	-0.4	-7.6	-26.6	-27.0	-10.1	-28.4	-31.2
harmonic frequencies (cm^{-1})	3627	3604	3422	3397	3428	3398	3540
	3550	3536	2764	3359	2395	3383	3394
	1976	1864	1577	1449	1646	488	1669
	776	823	1073	1100	1094	1070	1075
	635	623	1008	1060	813	1021	944
	46	216	690	904	628	932	317
	774	395i	395i	661	363	663	559
	634	760	501	220	323	319	216
		599	394	171	1377i	259i	744i
moments of inertia ($10^5\ m_ea_0{}^2$)	0.968	0.884	0.299	0.625	0.454	0.798	0.955
	14.11	3.285	4.287	3.024	3.864	2.112	2.317
	15.08	4.168	4.586	3.574	4.256	2.785	3.139

TABLE 3: Energies, Frequencies, and Moments of Inertia along the Entrance Channel Path for C + HCCH

	R1a	R1b	R1c	R1d	R1e	R1f	R1g path
energy (kcal/mol)	−5.7	−3.9	−2.3	−2.0	−1.8	−0.6	−0.4
harmonic frequencies (cm^{-1})	3621	3623	3625	3624	3625	3626	3627
	3548	3547	3548	3548	3549	3549	3550
	1942	1971	1975	1973	1974	1976	1976
	794	793	782	781	779	776	776
	634	176	92	72	62	635	635
	181	127	74	70	59	23	46
	769	781	777	638	637	774	774
	619	632	635	777	776	634	634
	128i	640	637		635		
moments of inertia ($10^5\ m_ea_0 2$)	0.932	0.954	0.961	0.966	0.969	0.968	0.968
	3.571	4.392	6.150	6.977	6.976	11.30	14.11
	4.503	5.346	7.111	7.943	7.944	12.27	15.08

cyclopropynylidene), with the calculations predicting that cyclic C_3H is about 1 kcal/mol more stable. The cyclic C_3H isomer is produced from a path that involves the cyclic C_3H_2 (min4) intermediate, while the linear isomer can be produced from two pathways (min3 and min5). All three reaction paths have min1 as a common precursor. Our calculations indicate that there are no exit channel barriers for the production of either product, so transition states associated with the final product formation

Reactions of C, CH, and $^1CH_2$ with Acetylene

J. Phys. Chem. A, Vol. 102, No. 29, 1998 **5859**

TABLE 4: Energies, Frequencies, and Moments of Inertia for Minima for CH + HCCH

	reactant	min1	min4	min5	min6 propargyl	min7	CH₂CC propargylene	C₃H₂
Structure								
Energy (kcal/mol)	0.0	-46.4	-29.4	-60.2	-107.2	-37.0	-8.9	-9.9
harmonic frequencies (cm⁻¹)	3627	3395	3388	3438	3602	3391	3297	3509
	1977	3363	3379	3324	3439	3387	3401	3504
	774	3357	3273	3279	3324	3302	2048	1495
	774	1465	1397	1587	2086	1398	1581	1251
	3550	1424	1275	1491	1557	1229	1148	661
	634	1123	1023	1168	1073	1151	1088	444
	634	958	983	1129	1054	1024	965	385
		930	676	991	516	905	259	359
	3058	849	664	813	478	856	202	150
		622	435	599	415	624		
		505	401	461	326	563		
		409	292	337	273	444		
moments of inertia (10^5 $m_ea_0^2$)		1.237	1.655	0.250	0.245	1.493		
		2.137	3.153	3.844	4.372	3.013		
		3.354	4.786	4.094	4.617	4.505		

TABLE 5: Energies, Frequencies, and Moments of Inertia for Saddle Points for CH + HCCH, Including One Point in the Entrance Channel (Labeled "path")

	path	sp1	sp3	sp4	sp5	sp6	sp7	sp8	sp9	sp10
Structure										
Energy (kcal/mol)	-1.9	-10.6	-30.2	-59.0	-26.3	-16.3	-17.0	-13.0	-8.6	10.4
harmonic frequencies (cm⁻¹)	3883	3623	3495	3460	3387	3404	3492	3422	3402	3492
	3548	3553	3444	3339	3380	3262	3204	3242	3297	3489
	2950	3071	3219	2837	3279	2762	2338	3131	2038	1473
	1951	1922	1574	1634	1386	1610	1734	1562	1580	1206
	736	922	1250	1567	1365	1267	1171	1262	1147	842
	452	812	1043	1175	940	1069	1079	1110	1088	609
	399	777	976	1031	924	959	997	941	958	442
	52	648	940	711	898	884	706	858	270	196
	715	631	760	591	857	787	580	796	225	668i
	518	236	755	498	532	583	479	580	164	
	302	270	1209i	389	311	357	347	359	131	
		330i	780i	460i	457i	393i	1154i	384i	553i	
moments of inertia (10^5 $m_ea_0^2$)	0.851	0.985	1.481	1.227	1.532	2.376	2.487	1.790	0.405	0.412
	8.767	4.291	2.308	3.358	2.700	3.409	3.502	3.700	7.637	3.196
	9.618	5.276	3.790	4.585	4.202	5.626	5.855	5.359	7.815	3.604

TABLE 6: Energies and Moments of Inertia along the Entrance Channel Path for CH + HCCH

	R2a	R2b	R2c	R2d	R2e	R2f path	R2g	R2h
energy (kcal/mol)	−6.9	−5.5	−4.3	−3.4	−3.1	−1.9	−1.2	−0.7
moments of inertia (10^5 $m_ea_0^2$)	1.004	1.010	1.009	0.996	0.977	0.851	0.814	0.908
	4.801	5.235	5.871	6.473	6.798	8.767	10.83	13.36
	5.805	6.245	6.880	7.469	7.775	9.618	11.65	14.27

steps were not determined. The properties of the minima in Figure 1a are very similar to those presented in the work by Ochsenfeld et al.[9] In particular, the energies of min1, min3, min4, and min5 are −32.2, −92.1, −50.9, and −59.9 kcal/mol in the Ochsenfeld calculation, compared to −29.0, −83.9, −45.3, and −57.0 kcal/mol in the present results. This is an encouraging agreement given that the computational methods used were quite different (CCSD(T) in Ochsenfeld, CASSCF-ICCI in the present calculations).

Stationary point energies, geometries, and frequencies for R2 and R3 were presented in ref 1. A summary that includes previously unpublished moment of inertia data is presented in

TABLE 7: Energies, Frequencies, and Moments of Inertia for Minima for CH$_2$ + HCCH

	reactant	min1	min2	min3 cyclo-propene	min4 allene	min5 methyl-vinylidene	min6 propyne
Structure							
Energy (kcal/mol)	0.0	-49.7	-42.5	-88.2	-112.1	-66.6	-113.7
harmonic frequencies (cm^{-1})	3627	3415	3364	3452	3395	3319	3603
	1977	3305	3322	3417	3361	3301	3298
	774	3283	3269	3309	3298	3292	3241
	774	3116	3078	3222	3067	3197	3001
	3550	1925	1521	1670	2006	1663	2226
	634	1657	1470	1577	1564	1583	1571
	634	1495	1228	1161	1488	1578	1535
		1355	1183	1122	1077	1494	1472
	3355	1272	1090	1109	1076	1192	1098
	3130	1082	1042	1091	1022	1092	1077
	1105	1049	878	1042	874	968	907
		984	861	934	840	928	559
		662	763	815	811	659	558
		456	630	772	322	254	292
		118i	585	570	282	204	287
moments of inertia (10^5 m$_e$a$_0^2$)		0.597	1.292	1.128	0.369	0.817	0.454
		3.357	2.311	2.662	4.471	3.506	4.211
		3.953	3.136	3.569	4.613	4.117	4.457

TABLE 8: Energies, Frequencies, and Moments of Inertia for Saddle Points for CH$_2$ + HCCH, Including One Point in the Entrance Channel (Labeled "path")

	path	sp0	sp1	sp1'	sp2	sp3	sp4	sp5	sp7
Structure									
Energy (kcal/mol)	-1.3	-10.8	-27.6	-32.4	-42.5	-42.8	-49.1	-30.2	-37.9
harmonic frequencies (cm^{-1})	3618	3628	3507	3463	3432	3422	3463	3395	3402
	3540	3556	3402	3437	3326	3416	3264	3376	3349
	3090	3211	3282	3311	3194	3318	2338	3276	3286
	1961	3121	2346	2315	2376	3287	1598	2450	3070
	1509	1942	1921	1811	1826	1612	1519	1602	1583
	778	1489	1536	1530	1545	1543	1220	1430	1517
	636	934	1075	1059	1206	1309	1113	1246	1202
	220	786	946	976	1071	1128	1004	1222	1129
	67	785	736	823	1040	1003	728	1124	1065
	3165	709	639	774	1019	914	3379	1056	1006
	781	642	610	683	726	826	1179	1022	964
	645	639	525	570	521	640	1036	842	929
	132	253	314	468	366	590	842	714	834
	117	230	159	298	346	356	643	348	663
		212	1091i	1359i	645	218i	1089i	805i	254i
moments of inertia (10^5 m$_e$a$_0^2$)	0.902	0.100	0.360	0.100	0.540	0.627	1.225	1.216	1.166
	11.90	1.100	4.455	0.262	3.874	3.875	2.775	2.191	2.833
	12.60	4.354	4.591	8.440	4.298	4.396	3.776	2.950	3.715

Tables 4 and 5 for R2 and Tables 7 and 8 for R3. Schematic drawings for these reaction paths are shown in Figure 1b,c. Here we use the labeling convention of ref 1 to identify the minima and saddle points. R2, like R1, has two possible products, but our calculations indicate that there is an exit channel barrier (sp10) for producing the cyclic C$_3$H$_2$ isomer. This should disfavor this product relative to the linear CH$_3$CC product.

Since the initial addition step for all three reactions is

Reactions of C, CH, and $^1CH_2$ with Acetylene

J. Phys. Chem. A, Vol. 102, No. 29, 1998 **5861**
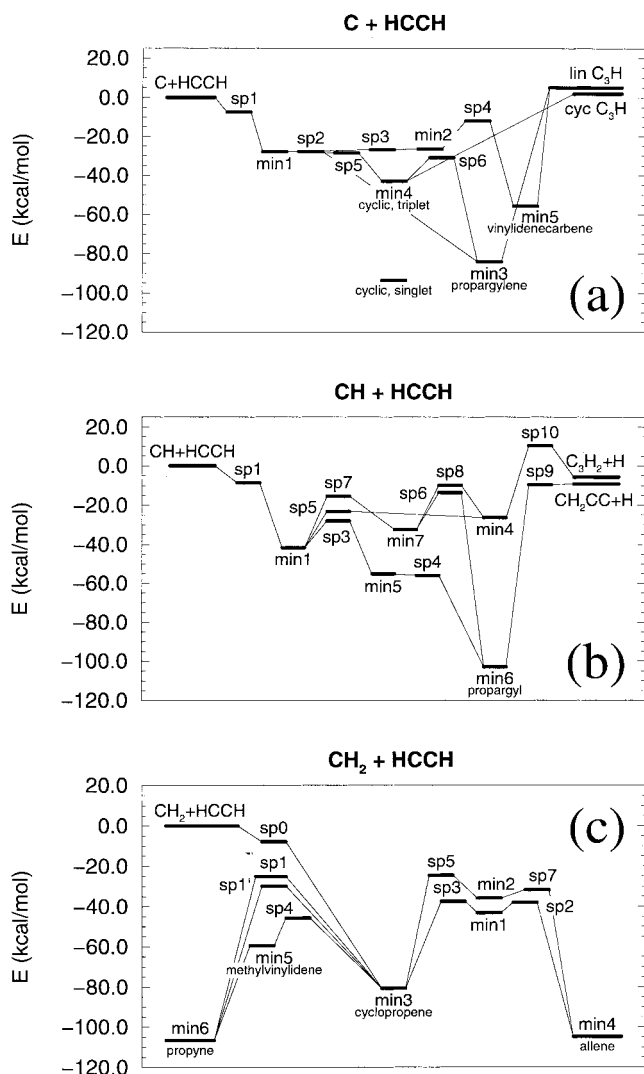
Figure 1. Schematic drawing of minimum energy paths: (a) C + HCCH, (b) CH + HCCH, (c) CH_2 + HCCH.

TABLE 9: Energies and Moments of Inertia along the Entrance Channel Path for CH_2 + HCCH

	R3a	R3b	R3c path	R3d
energy (kcal/mol)	−4.6	−2.5	−1.3	−0.8
moments of inertia ($10^5 \, m_e a_0^2$)	1.083	0.922	0.902	0.993
	6.020	9.479	11.90	14.02
	6.905	10.21	12.60	14.81

barrierless, it is essential to determine detailed information about the reaction paths for this step to determine rate constants. To do this, we determined energies, geometries, and frequencies at points along the minimum energy path for the initial addition step for R1 (Table 3). In addition, energies and geometries were calculated at points along the entrance channel for R2 and R3 (Tables 6 and 9). Note that frequencies were calculated only at one point in the entrance channel for R2 and R3 (labeled "path" in Tables 5 and 8). Determination of this point is described in part III.

III. RRKM Calculations

We use the reaction mechanisms shown in Figure 1 for the three reactions. In the figure, the nth transition state in a mechanism is labeled sp$n$ and the nth intermediate complex is labeled min$n$. The microcanonical rate constants for the forward and back reactions at the nth transition state are denoted as κ_n and κ_{-n}, respectively. For R1, the bottlenecks in the product

pathways are considered to be at infinite separation, and the microcanonical rate constants along these pathways are labeled κ_{lin} and κ_{cyc} for the linear and cyclic products, respectively.

Application of the steady-state approximation on all intermediate species yields (in the low-pressure limit) an effective microcanonical rate constant of the form

$$\kappa_{st} = \kappa_{path}(1 - \kappa_{eff}) \qquad (1)$$

where κ_{path} is the variational rate constant along the entrance channel reaction path.[14] κ_{eff} is a ratio involving all other microcanonical rate constants and, in this study, is nearly zero. The forms of κ_{eff} for the three reactions are

R1:

$$\kappa_{eff} = \frac{\kappa_{-path}}{C_1 - C_3}$$

$$C_1 = \kappa_{-path} + \kappa_2 + \kappa_3 + \kappa_5$$

$$C_2 = \frac{\kappa_3 \kappa_{-3}(\kappa_{-4} + \kappa_{lin})}{(\kappa_4 + \kappa_{-3})(\kappa_{-4} + \kappa_{lin}) - \kappa_4 \kappa_{-4}} \qquad (2a)$$

$$C_3 = C_2 + \left(\frac{\kappa_2 \kappa_{-2}}{\kappa_{-2} + \kappa_{-6} + \kappa_{lin}} + \kappa_{-5} \right)$$

$$\left[\frac{\kappa_5(\kappa_{-2} + \kappa_{-6} + \kappa_{lin}) + \kappa_2 \kappa_{-6}}{(\kappa_{-5} + \kappa_6 + \kappa_{cyc})(\kappa_{-2} + \kappa_{-6} + \kappa_{lin}) - \kappa_6 \kappa_{-6}} \right]$$

R2:

$$\kappa_{eff} = \frac{\kappa_{-path}}{C_1 - C_6}$$

$$C_1 = \kappa_{-path} + \kappa_3 + \kappa_5 + \kappa_7$$

$$C_2 = \kappa_{-4} + \kappa_{-6} + \kappa_9$$

$$C_3 = \left(\frac{1}{\kappa_{-7} + \kappa_6 + \kappa_8} \right)\left[\kappa_7 + \frac{\kappa_5 \kappa_{-8}}{\kappa_{-4} + \kappa_{-8} + \kappa_{10}} + \frac{\kappa_3 \kappa_4 \kappa_{-6}}{(\kappa_{-3} + \kappa_4)(C_2 - \kappa_4 \kappa_{-4})} \right]$$

$$C_4 = \left(\frac{1}{\kappa_{-7} + \kappa_6 + \kappa_8} \right)\left[\kappa_8 \kappa_{-8} + \frac{\kappa_4 \kappa_{-6}}{C_2(C_2 - \kappa_4 \kappa_{-4})} + \frac{\kappa_6 \kappa_{-6}}{C_2} \right]$$

$$C_5 = \left(\frac{C_3}{1 - C_4} \right)\left(\frac{\kappa_{-3} \kappa_{-4} \kappa_6}{C_2 - \kappa_4 \kappa_{-4}} + \frac{\kappa_{-4} \kappa_8}{\kappa_{-4} + \kappa_{-8} + \kappa_{10}} + \kappa_{-7} \right) \qquad (2b)$$

$$C_6 = C_5 + \frac{C_2 \kappa_3 \kappa_{-3}}{(\kappa_{-3} + \kappa_4)(C_2 - \kappa_4 \kappa_{-4})} + \frac{\kappa_{-4} \kappa_5}{\kappa_{-4} + \kappa_{-8} + \kappa_{10}}$$

R3:

$$\kappa_{eff} = \frac{\kappa_{-path}}{C_1 - C_2}$$

$$C_1 = \kappa_{-path} + \kappa_1 + \kappa_{1'} + \kappa_3 + \kappa_4 + \kappa_5 \qquad (2c)$$

$$C_2 = \frac{(\kappa_3)^2}{\kappa_{-3} + \kappa_2} + \frac{(\kappa_5)^2}{\kappa_{-5} + \kappa_7}$$

We use variational RRKM theory[15] based on a modified version of the code developed by W. L. Hase and D. L. Bunker[16] to calculate the microcanonical rate constants. The Whitten–Rabinovitch approximation is used to calculate the numbers of states of the transition states and the densities of states of the

complexes. The RRKM expression for the microcanonical rate constant is

$$\kappa(E^*) = \frac{N(E^{\ddagger})}{h\rho(E^*)} \tag{3}$$

where N is the number of states at the transition state and ρ is the density of states of the initial complex. The canonical rate constant is given by

$$\kappa(T) = \frac{1}{Q_{reag}} \int \sum_{J,K} (2J+1)\kappa_{st} e^{-E/k_B T} \rho_{reag} \, dE \tag{4}$$

where ρ_{reag} and Q_{reag} are the density of states of the reagents and the reagent partition function, respectively. J and K are the total angular momentum quantum number and its body-fixed projection. Both J and K are assumed to be conserved, which means that the same J and K are used in evaluating κ_{st} and ρ. In the results to be presented, we have calculated the canonical rate constant at 300 and 1000 K, by evaluating the integral in eq 4 numerically using the trapezoid rule (with an error of $<1 \times 10^{-4}$). Maximum J and E values used are 60 and 5 kcal/mol at 300 K and 99 and 35 kcal/mol at 1000 K.

To study the pressure dependence of the rate constants, we have calculated unimolecular lifetimes of the intermediate complexes. The lifetime τ_n of the nth intermediate complex is

$$\frac{1}{\tau_n} = \sum_i \kappa_i \tag{5}$$

where the κ_i's are the microcanonical rate constants (averaged over J and K) of all steps in the mechanism in which the nth complex (min$n$) is the reacting species. A branching fraction for the products in R2 was also calculated. Branching fractions for R1 and R3 could not be found because characteristics along the exit channels were not available.

Since all three reactions have barrierless initial addition pathways, we use a variational method to determine κ_{path}.[14] According to variational theory, the bottleneck of a reaction occurs at the point along the minimum energy path where the number of states available, and hence the microcanonical rate constant, is at a minimum. This means that calculations are done at various points along the minimum energy path until a minimum in the rate is found, thereby defining the reactive bottleneck. For R1, we calculated rate constants for all the ab initio geometries in Table 3, and we found that the minimum in the rate constant is at the highest energy point. To check if this is indeed the minimum, we extrapolated points between -0.4 and 0.0 kcal/mol. This was accomplished by fitting energies and frequencies of the reactants, sp1, and the point at -0.4 kcal/mol to exponentials of the form

$$\nu = \nu_0 + a e^{-br} \tag{6a}$$

$$E = E_0 + a e^{-br} \tag{6b}$$

where r is the distance between the attacking carbon atom and the acetylenic carbon to which it bonds. The rate constants $k(T)$ for both the ab initio points and the extrapolated points are shown in Figure 2 as a function of the energy along the reaction path. This figure shows that indeed the minimum rate constant is associated with the highest energy point.

For R2 and R3, only energies and geometries were determined along the entrance channel reaction path. Frequencies were
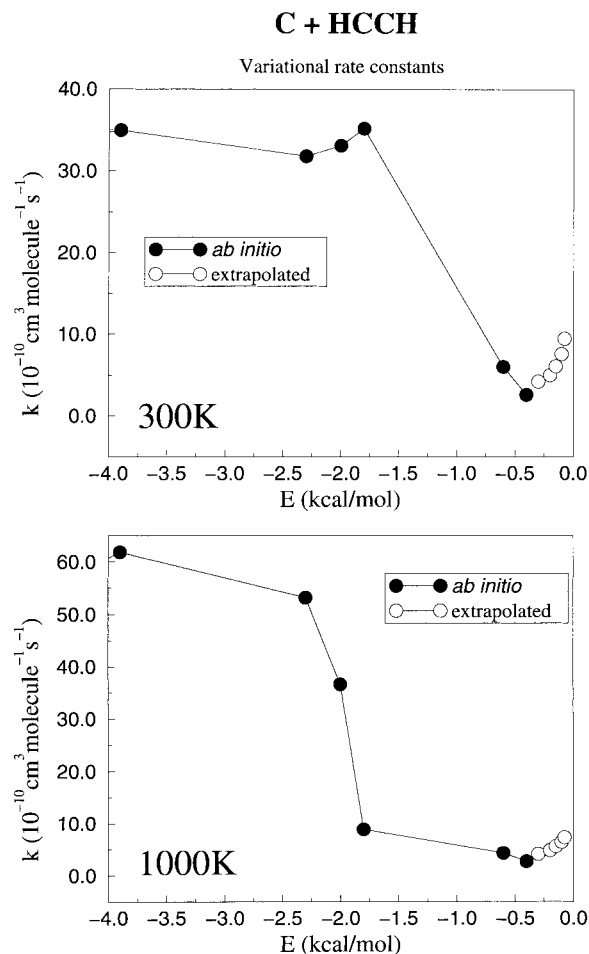
Figure 2. Variational rate constant vs reaction path energy for C + HCCH.

approximated by two methods. One involved fitting known frequencies of the reactants, sp1, and min1 to an exponential of the form mentioned above, eq 6a. The second involved linearly fitting known frequencies at reactants and sp1 by

$$\nu = \nu_0 + ar \tag{7}$$

In both cases, r is again the distance between the two carbon atoms in the reactants that form a new bond. Rate constants for R2 and R3 at each point along the reaction path for both fitting methods are shown in Figures 3 and 4. Inspection of the results reveals that the value of the rate constant is very sensitive to the method used to fit the frequencies and, therefore, to the values of the frequencies. A more accurate determination of the frequencies was therefore instituted.

Since the minimum rate constant, although very different in both interpolation methods, occurs at about the same geometry, ab initio frequencies were calculated at these chosen geometries. The rate constant was then recalculated with the ab initio frequencies. This new value is also shown in Figures 3 and 4. The best values for all three reactions along with experimental numbers[17-24] are presented in Table 10. Lifetimes of complexes are given in Tables 11–13.

IV. Results and Discussion

The rate constants for all reactions agree quite well with the experimental numbers. In view of the uncertainty associated with finding the minima in Figures 2–4, the calculated values easily have 50% uncertainty associated with them, so within

Reactions of C, CH, and ^{1}CH$_2$ with Acetylene

J. Phys. Chem. A, Vol. 102, No. 29, 1998 **5863**

CH + HCCH

Variational rate constants

CH$_2$ + HCCH

Variational rate constants
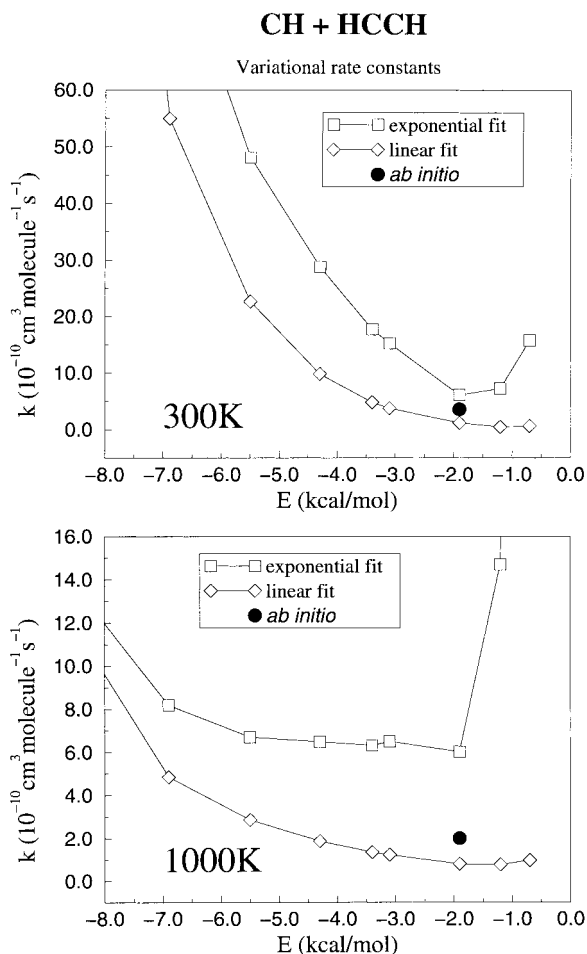
Figure 3. Variational rate constant vs reaction path energy for CH + HCCH.

Figure 4. Variational rate constant vs reaction path energy for CH$_2$ + HCCH.

those error bars we match all the recent measurements. The temperature dependence of the rate constant cannot be determined experimentally for R1 and R3, since all measurements were made at 300 K. For R2, a slightly negative dependence is apparent in the experiments done by Thiesemann et al.[18] and Berman et al.[19] This is the expected result for a barrierless reaction. The RRKM results for R2 and R3 also show a negative dependence. However, the difference in the values at 300 and 1000 K for R2 and R3 may be exaggerated due to the uncertainty in the minima. For R1, we see no temperature dependence, but again there is a significant uncertainty in the result.

Note that the calculated rate constants are for the low-pressure limit, while it is not clear if this is the case for the measurements. At high enough pressures, collisional stabilization of intermediates is expected, and the effective rate constant should increase. The pressure dependence of the rate constants can be estimated as discussed by Harding et al.,[25] but the formulation requires determining collisional stabilization rates for each c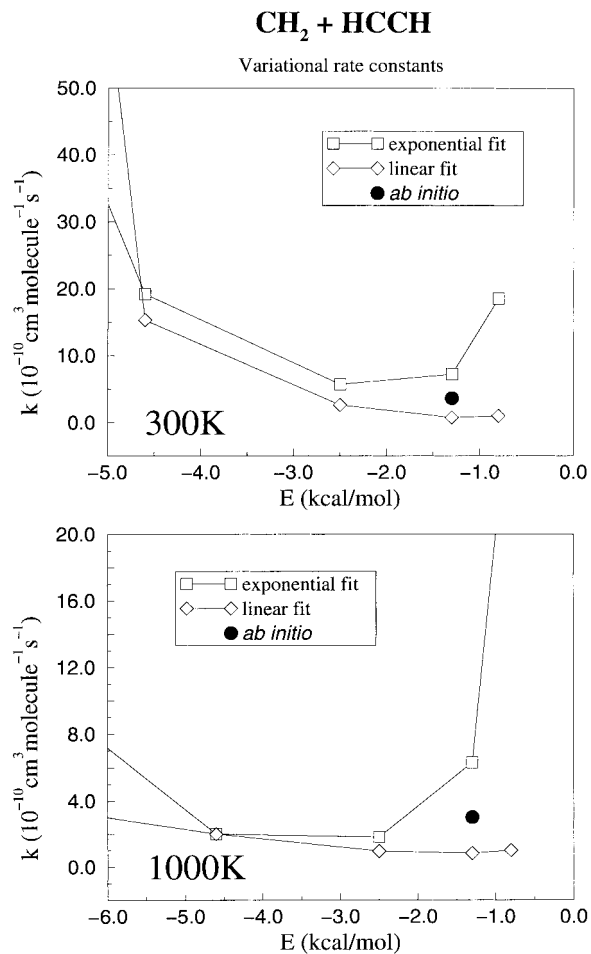omplex as an additional step in the reaction mechanism. The importance of collisional stabilization depends on the value of $\omega\tau$ for each complex, where τ is the unimolecular lifetime of the complex and ω is the effective collision frequency with bath gases. ω has the form

$$\omega = \beta(T) Z(T) P \tag{8}$$

where $\beta(T)$ is the collision efficiency of the third body, $Z(T)$ is the gas kinetic collision frequency, and P is the pressure. The collision frequency can be calculated with the standard for-

TABLE 10: Rate Constants for Reactions with Acetylene, Including Experimental Values

reactant	temperature (K)	pressure (Torr)	$k(T)$ (10^{-10} cm^3 molecule^{-1} s^{-1})	ref
C(^{3}P)	300		2.6	this work
	1000		2.7	this work
	300	2	2.0 ± 0.1	17
CH(X$^2\Pi$)	300		3.6	this work
	1000		2.0	this work
	289	8	3.82 ± 0.08	18
	291	100	3.12 ± 0.05	18
	1000	100	2.5 ± 0.2	18
	297	100	4.2 ± 0.2	19
	1000	100	3.7 ± 0.4	19
	298	100	2.2 ± 0.4	20
	298		0.75 ± 0.15	21
^{1}CH$_2$	300		3.6	this work
	1000		3.0	this work
	295	15	3.5 ± 0.7	22
	298	4	2.93 ± 0.19	23
	298	0.75	2.9^a	24

^{a} Calculated from total rate constant including reaction to ^{3}CH$_2$ reported at 3.7 ± 0.3 and branching ratio for formation of ^{3}CH$_2$ reported at 0.22.

mula.[26] However, $\beta(T)$ is an empirical variable and must be estimated, usually with reference to an experimental value for the rate constant at high pressure. However, all experimental values of the rate constant available presently were measured at or near the low-pressure limit. As a result, any estimate of $\beta(T)$ will be somewhat arbitrary.

The results in Tables 11−13 suggest that two species have

5864 *J. Phys. Chem. A, Vol. 102, No. 29, 1998*

Guadagnini et al.

TABLE 11: Complex Lifetimes for C + HCCH (in ps)

complex	τ (300 K)	τ (1000 K)
min1	3.1×10^{-2}	3.4×10^{-2}
min1p	6.4×10^{-2}	6.4×10^{-2}
min2 propargylene	2.5×10^{3}	1.9×10^{3}
min3 cyclic	47.7	53.6
min4	4.4×10^{-2}	4.1×10^{-2}

TABLE 12: Complex Lifetimes for CH + HCCH (in ps)

complex	τ (300 K)	τ (1000 K)
min1	1.5	1.4
min4	0.4	0.4
min5	0.03	0.02
min6 propargyl	28.1	24.8
min7	2.3	1.8

TABLE 13: Complex Lifetimes for CH$_2$ + HCCH (in ps)

complex	τ (300 K)	τ (1000 K)
min1	0.17	0.16
min2	5.1×10^{-3}	5.0×10^{-3}
min3 cyclopropene	3.7	4.1
min4 allene	4.0×10^{2}	4.4×10^{2}
min5 methylvinylidene	1.9	2.0
min6 propyne	2.5×10^{3}	2.4×10^{3}

long enough lifetimes (>1 ns) to show pressure effects at 100 Torr, i.e., propargylene and propyne. However in both cases, the reactions we are studying can occur by other pathways that involve short-lived intermediates and low barriers. We conclude therefore that the pressure dependence of the rate constants should be weak for $P \leq 100$ Torr.

In the present study, only the triplet surface for R1 is considered. Takahashi et al.[43] also include ab initio calculations for the singlet surface. They postulate a mechanism for reaction that includes surface hopping and formation of a singlet intermediate analogous to min4 (as plotted in Figure 1a). However, their calculation of the triplet surface shows a large barrier for reaction, whereas the present calculation shows no barrier. Due to the small probability expected for surface crossing[27] and the fact that there is no barrier on the triplet surface, we believe the singlet surface to be unimportant. This assumption is supported by the RRKM rate constant, which agrees quite well with experiment despite exclusion of the singlet surface.

The branching ratio for the products of R2, CH$_2$CC:C$_3$H$_2$, is essentially 1:0. This is not surprising considering the saddle point for reaction to C$_3$H$_2$ is more than 10 kcal/mol above the reagent energy, whereas that for CH$_2$CC is 10 kcal/mol below. Therefore, CH$_2$CC (propargylene) is expected to be the major product of the reaction between CH and acetylene. This is significant since both propargyl and propargylene can dimerize with no barrier to form six-member rings.[1]

Very recently,[11] Vereecken and co-workers have presented a detailed study of reaction R2 using a density functional based method (B3LYP/6-31G**). Many of their results are similar to those presented in Figure 1b, but there are also important differences. Both calculations agree that the initial addition mechanism is barrierless and can produce min1, but Vereecken suggests that there are other addition pathways, including one that forms min6 directly from the reactants. The properties of these initial addition pathways were not discussed. However they also find that there are other pathways for forming products, although none of them involve species as stable as min6. We have not extended our calculations to study these additional pathways for reaction, but we note that only min6 has a lifetime that is long enough to be of interest in pressure-dependent

studies for pressures below 100 Torr. Vereecken et al. did not estimate rate constants from their results, so at this point it is not possible to make quantitative comparisons with our results or experiment.

Recent isotope effect measurements concerning reaction R2[18] suggest that the rate-determining transition state for this reaction cannot be loose and cannot involve participation of significant hydrogen atom motion associated with the acetylenic hydrogen atoms. The properties that we find for the structure labelled "path" in Tables 5 and 6 are consistent with this conclusion. In particular, we find that the frequencies in Table 5 can be divided into two groups, namely, those associated with the acetylene vibrations and the CH stretch which are not strongly perturbed from their reagent values in Table 4 and those associated with transitional modes (the two lowest frequencies) which are still high enough to consider the transition state to be tight rather than loose. This provides qualitative evidence in favor of the transition-state properties that we find, although we have not performed detailed isotope effect calculations to see if this also works quantitatively.

Molecular beam experiments reported by Kaiser et al.[10,11,28] for R1 have shown predominantly forward scattering at low energy and then symmetrical forward and backward scattering at higher energies. They conclude that this behavior arises from the contribution of two different *direct* reaction mechanisms, whose relative importance varies with energy, with the lower energy mechanism leading to cyclic C$_3$H formation and the higher energy mechanism involving linear C$_3$H formation through a geometrically symmetrical intermediate. They disregard complex formation as a possible explanation for either mechanism, as they believe that the lifetimes of the complexes are shorter than the rotational lifetimes. The rotational lifetime can be estimated in the present work by equating the classical and quantal forms of the rotational energy, giving the equation $\hbar j \cong I\omega$.[29] Here j is the rotational quantum number, ω the angular velocity, and I the moment of inertia. Given the rotational constant $B = \hbar^2/2I$, and $\omega = jB/\hbar$, the rotational lifetime can be written as $\tau_r \cong 4\pi I/j\hbar$. To maximize τ_r, we use $j = 1$ and $I = 5 \times 10^5 \, m_e a_0^2$, which is an upper bound on the moments of inertia of all complexes reported in Table 1. These give a value $\tau_r \cong 44$ ps. Values of the lifetime of propargylene calculated in this study are on the order of 10 times longer than this at 300 K, suggesting that complex formation should be important if the reaction behaves statistically. In fact, we should further note (see discussion at the end of this section) that anharmonic corrections are likely to increase the lifetimes relative to what we have calculated. This would therefore seem to be at odds with the experimental angular distributions. This could happen if the intermediate complexes did not exhibit statistical behavior; however, this seems unlikely given the depth of the wells and absence of high barriers between the different minima. Another possibility is that the barriers are inaccurate, and propargylene is not accessible to low-energy collisions. This would allow more direct reaction pathways, such as min4 dissociation into cyclic C$_3$H, to dominate at low energies, which is what Kaiser et al. postulate. Unfortunately it is not possible for us to say anything more definitive about these experiments.

For R1 and R3, details about the minimum energy reaction path from the complexes to products were not determined, and the calculated lifetimes of the complexes do not include contributions for pathways to products. However, it is not expected that these pathways should contribute significantly to the lifetime, as the number of states near the products is very small in comparison to the numbers of states at all other

Reactions of C, CH, and $^1CH_2$ with Acetylene

J. Phys. Chem. A, Vol. 102, No. 29, 1998 **5865**

available saddle points. To verify that this is true, we calculated the lifetimes for complexes for R2 both including and excluding the product pathways. We found that excluding the pathway for reaction of propargyl to products changed the lifetime of the propargyl radical only in the fourth decimal place. There was no change in the lifetime for min4. Considering this, we feel that the lifetimes of R1 and R3 should be unaffected by excluding the product pathway.

There are four possible sources of error inherent in the present calculations (other than errors in the potential energy surfaces): errors involving the steady-state approximation, transition-state theory, neglect of anharmonicity, and neglect of quantum corrections. For all three reactions, substitution of the definition of all RRKM rate constants into eq 2 and subsequent algebraic reduction results in equivalent equations involving only the numbers of states at the saddle points. All densities of states of the complexes cancel as dictated by the steady-state approximation. Entering the values of the numbers of states as calculated by the Hase code into the equation gives a κ_{eff} that is essentially zero. Consequently, the steady-state approximation attributes the rate-limiting step to the entrance channel bottleneck. Considering that all other saddle points are well below the reagent energy, the number of states available at those points is much greater than the number available at the bottleneck and is expected to have much less influence on the rate constant. Therefore, the steady-state approximation should cause no significant error in the value of the rate constant.

Transition-state theories usually assume that the reaction bottleneck is determined by vibrationally adiabatic barriers along the minimum energy path. Once the barrier at the bottleneck is crossed, it is assumed that the system does not recross the barrier and return to reactants. If recrossing does occur, the true rate constant would be smaller than that calculated using transition-state theory. In all cases presented here, the bottleneck is below the reagent energy, and there is no true barrier. Once the reaction passes the bottleneck, a relatively stable complex is formed, so recrossing is expected to be minimal.

Anharmonic effects should lead to an increase in both the densities of states of the complexes and the numbers of states at the transition states.[30] For the rate constant, only the number of states at the bottleneck is important. Since there is little energy available at the bottleneck, anharmonic effects should not play an important role. As for the calculated lifetimes, the increase in the density of states of the complex due to anharmonicity should be larger than the corresponding increase in the numbers of states at the transition states since more energy is available to the complex. Neglecting anharmonicity will therefore result in lifetimes that are shorter. The calculated harmonic lifetime should then be considered as a lower bound.

Quantum corrections, such as zero-point corrections and tunneling, should not pose a problem, as there is no barrier to reaction, and all but one transition state is below reagent energy.

V. Conclusions

We report reaction pathways and energetics for the reaction of C(^3P) with acetylene. Furthermore, details along the entrance channel for addition of C, CH, and $^1CH_2$ with acetylene are reported. All three reactions proceed with no barrier. Potential surface data reported here and by Walch are used to calculate rate constants and lifetimes using variational RRKM theory. The rate constants and lifetimes calculated suggest that all three reactions could play important roles in interstellar and combustion chemistry. The rate constants are in good agreement with experimental values, and the negative temperature dependence

is as expected for barrierless reactions. Although not reported, the pressure dependence could be modeled using the results presented here if more experimental data were available. The lifetimes of complexes reported are long enough to give statistical behavior for experiments where complex formation can occur. Since the rate-limiting step for all three reactions is the initial addition step, it cannot be determined from comparisons of our results with available experiments whether the mechanisms involve complex formation or direct reaction. Further experiments or dynamical studies would need to be done to distinguish which mechanism is more important.

Supporting Information Available: Geometrical information is presented for the structures in Tables 1−3, 6, and 9 (6 pages). Ordering information is given on any current masthead page.

References and Notes

(1) Walch, S. P. *J. Chem. Phys.* **1995**, *103*, 7064.

(2) Miller, J. A.; Kee, R. J.; Westbrook, C. *Annu. Rev. Phys. Chem* **1990**, *41*, 345.

(3) (a) Baulch, D. L.; Cobos, C. J.; Cox, R. A.; Esser, C.; Frank, P.; Just, T.; Kerr, J. A.; Pilling, M. J.; Troe, J.; Walker, R. W.; Warnatz, J. *J. Phys. Chem. Ref. Data* **1992**, *21*, 411. (b) Miller, J. A.; Kee, R. J.; Westbrook, C. *Annu. Rev. Phys. Chem* **1990**, *41*, 345. (c) Boullart, W.; Devriendt, K.; Borms, R.; Peeters, J. *J. Phys. Chem.* **1996**, *100*, 998. (d) Gaydon, A. A.; Wolfhard, H. G. *Flames*; Wiley: New York, 1979. (e) Fenimore, C. P. In *Thirteenth Symposium (International) on Combustion*; Fenimore, C. P., Ed.; The Combustion Institute: Pittsburgh, PA, 1971; p 373. (f) Miller, J. A.; Bowman, C. T. *Prog. Energy Combust. Sci.* **1989**, *15*, 289.

(4) Takahashi, J.; Yamashita, K. *J. Chem. Phys.* **1996**, *104*, 6613.

(5) (a) Clary, D. C.; Haider, N.; Husain, D.; Kabir, M. *Astrophys. J.* **1994**, *422*, 416. (b) Bettens, R. P. A.; Lee, H. H.; Herbst, E. *Astrophys. J.* **1995**, *443*, 664. (c) Liao, Q.; Herbst, E. *Astrophys. J.* **1995**, *444*, 694. (d) Wayne, R. P. *Chemistry of Atmospheres*; 2nd ed.; Clarendon Press: Oxford, 1991.

(6) (a) Kern, R. D.; Chen, H.; Kiefer, J. H.; Mudipalli, P. S. *Combust. Flame* **1995**, *100*, 177. (b) Alkemade, U.; Homann, K. H. *Z. Phys. Chem. (Munich)* **1989**, *116*, 19. (c) Kern, R. D.; Singh, H. J.; Wu, C. H. *Int. J. Chem. Kinet.* **1988**, *20*, 731. (d) Wu, C. H.; Kern, R. D. *J. Phys. Chem.* **1987**, *91*, 6291. (e) Hurd, C. D.; Macon, A. R.; Simon, J. I.; Levetan, R. V. *J. Am. Chem. Soc.* **1962**, *84*, 4509.

(7) Westmoreland, P. W.; Dean, A. M.; Howard, J. B.; Longwell, J. P. *J. Phys. Chem.* **1989**, *93*, 8173.

(8) (a) Goodings, J. M.; Tanner, S. D.; Bohme, D. K. *Can. J. Chem.* **1982**, *60*, 2766. (b) Kistiakowsky, G. B.; Michael, J. V. *J. Chem. Phys.* **1964**, *40*, 1447.

(9) Kiefer, J. H.; Kumaran, S. S.; Mudipalli, P. S. *Chem. Phys. Lett.* **1994**, *224*, 51.

(10) Ochsenfeld, C.; Kaiser, R. I.; Lee, Y. T.; Suits, A. G.; Head-Gordon, M. *J. Chem. Phys.* **1997**, *106*, 4141.

(11) Kaiser, R. I.; Ochsenfeld, C.; Head-Gordon, M.; Lee, Y. T.; Suits, A. G. *Science* **1996**, *274*, 1508.

(12) Vereecken, L.; Pierloot, K.; Peeters, J. *J Chem. Phys.* **1998**, *108*, 1068.

(13) Walch, S. P. To be published.

(14) (a) Truhlar, D. G.; Gordon, M. S. *Science* **1990**, *249*, 491. (b) Liu, Y.-P.; Lu, D.-h.; Gonzalez-Lafont, A.; Truhlar, D. G.; Garrett, B. C. *J. Am. Chem. Soc.* **1993**, *115*, 7806.

(15) Robinson, P. J.; Holbrook, K. A. *Unimolecular Reactions*; Wiley-Interscience: London, 1972.

(16) Hase, W. L.; Bunker, D. L. *QCPE 234*; *Acc. Chem. Res.* **1983**, *16*, 258.

(17) Haider, N.; Husain, D. *J. Photochem. Photobiol. A: Chem.* **1993**, *70*, 119.

(18) Thiesemann, H.; MacNamara, J.; Taatjes, C. A. *J. Phys. Chem. A* **1997**, *101*, 1881.

(19) Berman, M. R.; Fleming, J. W.; Harvey, A. B. *Chem. Phys.* **1982**, *73*, 27.

(20) Butler, J. E.; Fleming, J. W.; Goss, L. P.; Lin, M. C. *Chem. Phys.* **1981**, *56*, 355.

(21) Bosnali, M. W.; Perner, D. *Z. Naturforsch.* **1971**, *26a*, 1768.

(22) Adamson, J. D.; Morter, C. L.; DeSain, J. D.; Glass, G. P.; Curl, R. F. *J. Phys. Chem.* **1996**, *100*, 2125.

(23) Hayes, F.; Gutsche, G. J.; Lawrance, D.; Staker, W. S.; King, K. D. *Combust. Flame* **1995**, *100*, 653.

(24) Hack, W.; Koch, M.; Wagner, H. G.; Wilms, A. *Ber. Bunsen-Ges. Phys. Chem.* **1988**, *92*, 674.

(25) Harding, L. B.; Wagner, A. F.; Bowman, J. M.; Schatz, G. C.; Christoffel, K. *J. Phys. Chem.* **1982**, *86*, 4312.

(26) (a) Keil, D. G.; Lynch, K. P.; Cowfer, J. A.; Michael, J. V. *Int. J. Chem. Kinet.* **1976**, *8*, 825. (b) Chan, S. C.; Bryant, J. T.; Spicer, L. D.; Rabinovitch, B. S. *J. Phys. Chem.* **1970**, *74*, 2058.

(27) Turro, N. J. *Modern Molecular Photochemistry*; University Science Books: Mill Valley, CA, 1991.

(28) Kaiser, R. I.; Ochsenfeld, C.; Head-Gordon, M.; Lee, Y. T.; Suits, A. G. *J. Chem. Phys.* **1997**, *106*, 1729.

(29) Levine, R. D.; Bernstein, R. B. *Molecular Reaction Dynamics and Chemical Reactivity*; Oxford University Press, Inc.: New York, 1987.

(30) Peslherbe, G.; Hase, W. L. *J. Chem. Phys.* **1994**, *101*, 8535.s